Spring 5-2020

Enhancing Upconversion nanoparticle performance of NaYF4: Yb,Tm with doping optimization and shell addition and of NaYF4: Yb,Er with Yb,Nd shell addition

Ashleigh M. Chov
University of South Dakota

Recommended Citation

Enhancing Upconversion nanoparticle performance of NaYF$_4$: Yb,Tm with
doping optimization and shell addition and of NaYF$_4$: Yb,Er with Yb,Nd shell addition

by

Ashleigh Chov

A Thesis Submitted in Partial Fulfillment
Of the Requirements for the
University Honors Program

_____

Department of Chemistry
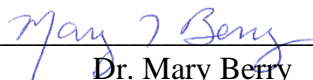The University of South Dakota
May 2020

1

The members of the Honors Thesis Committee appointed
to examine the thesis of Ashleigh Chov
find it satisfactory and recommend that it be accepted.

_____
Dr. Stanley May
Emeritus Professor of Chemistry
Director of the Committee

_____
Dr. Aravind Baride
Research Assistant Professor of Chemistry

_____
Dr. Mary Berry
Emeritus Professor of Chemistry

i

ABSTRACT

Enhancing Upconversion nanoparticle performance of NaYF$_4$: Yb,Tm with
doping optimization and shell addition and of NaYF$_4$: Yb,Er with Yb,Nd shell addition
Ashleigh Chov

Director: Dr. Stanley May

Upconversion (UC), is a phenomenon that occurs when low-energy excitation
(usually near-infrared (NIR)) results in higher-energy emission. Upconversion
nanoparticles (UCNPs) are particles less than 100 nm in size that are synthesized using
rare earth metals such as Yb, Er, Tm, and Y. UCNPs have important applications in a
variety of fields, including bio-imaging, security printing, and latent fingerprint
development. Traditional methods for latent fingerprint development such as fluorescent
powder dusting have several drawbacks including low contrast, high background
interference, and autofluorescence. NIR-to-NIR UCNPs are composed of NaYF$_4$: Yb,
Tm and emit 800 nm light under 980 nm excitation due to the absorbance of Yb^{3+} ions.
NIR excitation produces no background emission from substrates and ambient lighting
does not hinder the collection of the 800 nm emission from the nanoparticles. Exciting
using NIR light reduces fluorescence from the substrate and improves the contrast of
luminescent images created using the particles. These features make NIR-to-NIR UCNPs
attractive for latent fingerprint development. Here, NIR-to-NIR UCNPs of various Yb
doping with passive shell layers of NaYF$_4$ were synthesized. Passive shells are those that
do not participate in upconversion but assist in covering surface defects that may have
occurred during synthesis and decreases the effect of surface quenching. The goal of this
research was to optimize and increase the brightness of the NIR-to-NIR UCNPs by
adjusting the doping concentrations of Yb, while also observing the effect of surface

quenching before and after the addition of the inert $NaYF_4$ shells to the UCNPs. The brightness of the nanoparticles was analyzed using internal quantum efficiency measurements at varying excitation power densities. In addition to the NIR-to-NIR UCNPs, NIR-to-Green UCNPs with both an active shell of 10% Yb and 10% Nd and passive shell of $NaYF_4$ were synthesized. NIR-to-Green UCNPs are composed of $NaYF_4$: Yb, Er, and convert NIR excitation to shorter-wavelength green emission. The 980 nm excitation wavelength required by traditional Yb, Er UCNPs overlaps a weak absorbance band of water, interfering with excitation and increasing the chance of overheating tissues while imaging. However, addition of the active shell allows for the NIR-to-Green UCNPs to be excited by either 800 nm or 980 nm light while also covering surface defects and decreasing surface quenching. Exciting the particles with 800 nm, which is in a transparency window for biological samples, greatly reduces the danger of overheating tissue while maintaining the high penetration depth for bio-imaging. For security printing, these particles can also be used to print two different but overlapping images which can be viewed individually using different excitation sources.

Key Words: Upconversion, Passivation Layers, Nanoparticles, and Lanthanides

TABLE OF CONTENTS

LIST OF FIGURES

ACKNOWLEDGEMENTS

I would like to give a special thanks…

To Department of Chemistry: for allowing me to explore my interest in chemistry research through REUs, for the support they have given me throughout my time at USD.

To Dr. Stanley May: From the beginning of my college career, you have always provided me with continuous support and advice towards my endeavors at USD. I want to thank you for taking me into the May-Berry Laser Squad, the opportunities you have provided me to showcase my research at local, regional, and national meetings, and most of all for being my mentor.

To Dr. Aravind Baride: For teaching me the ropes of the Laser Lab, your patience, and encouraging me to challenge myself in lab. I can truthfully say that I have enjoyed every day I was in lab working under your care.

To the remainder of the May-Berry Laser Squad: Working with all of you has been a joy. You have all taught me so much not only about chemistry, but also about myself.

To my roommates: I could not have done this without you. No, seriously. Without the consistent moral and emotional support I have received from all of you, I would not have been able to make it this far. I will never forget the memories we have made, the countless hours in the library, or our Just Dance parties! If I would not have met any of you, I would not be the person I am today. All of you allowed me to be myself and accepted me for who I am. I will be forever grateful that USD and chemistry brought (most of) us together.

CHAPTER 1. INTRODUCTION

As with any research project, it is crucial to understand the big picture. This gives the project focus and meaning. In this chapter, the motivation to synthesize and optimize UCNPs along with the basic principles of the process are explained.

Latent fingerprints are fingerprints that are not visible to the naked eye. At a crime scene, fingerprints can be one of the most crucial and incriminating pieces of evidence. The methods that are used for fingerprinting often lack the level of detail on fine features such as sweat pores and ridge detail that would make identification more efficient and reliable. One of the most common methods for developing latent fingerprints is with fluorescent powders. Fluorescent powders are down-conversion phosphors, meaning that the energy of the excitation light (usually UV) is higher than that of the emitted light (usually visible). Down-conversion powders are helpful in situations where the fingerprint is on a substrate that has little background fluorescence. However, many substrates fluoresce under UV excitation. In addition, cameras used to take these fingerprint images are not very sensitive to the emission coming from the fluorescent powers, which results in poor quality images. Upconversion (UC), on the other hand, is a phenomenon that occurs when low-energy excitation (usually NIR) results in higher-energy emission. It is the successive absorption of two or more photons and results in the emission of a single high energy photon. This process is nonlinear and is a result of multiple energy-transfer events from Yb^{3+} ions to either Tm^{3+} ions (for NIR-to-NIR upconversion) or Er^{3+} ions (for NIR-to-Green upconversion).

To utilize this process for the purpose of latent fingerprint development, rare earth metals are used for the synthesis of the UCNPs. $NaYF_4$ particles doped with Yb and Tm are called NIR-to-NIR UCNPs, because they convert NIR excitation (980nm) to shorter-wavelength NIR emission (800 nm) (see Figure 1). The Yb^{3+} ions act as a sensitizer, the ion that absorbs the excitation energy (980 nm). The energy absorbed by the Yb^{3+} ions is then transferred to nearby Tm^{3+} activator ions, which are responsible for the upconversion emission of interest. It is imperative that the sensitizer and activator ions have similarly spaced intermediate excited states to ensure efficient energy transfer. In the case of NIR-to-NIR UCNPs, the activator within the system is Tm^{3+} ions. An incoming photon of energy is absorbed by a Yb^{3+} ion which then transfers the energy to a nearby Tm^{3+}, the transferred energy is stored within the Tm^{3+} ion long enough for a Yb^{3+} ion to absorb another incoming photon and the Yb→Tm transfer to occur once again. This results in a buildup of energy within the Tm^{3+} ion promoting the Tm^{3+} ion to higher and higher energy levels. The energy relaxation can result in 650 nm red ($^1G_4 \rightarrow {}^3F_4$), 475 nm blue ($^1G_4 \rightarrow {}^3H_6$), 450 nm blue ($^1D_2 \rightarrow {}^3F_4$), and 800 nm NIR ($^3H_4 \rightarrow {}^3H_6$) emission. By applying β-$NaYF_4$: Yb, Tm upconversion nanoparticles to latent fingerprints, we can capture images in the NIR region, corresponding to the 800 nm upconversion emission.

The β-$NaYF_4$: Yb, Tm NIR-to-NIR upconversion nanoparticles are dusted onto a substrate in order to identify the presence of latent fingerprints. The substrate is then excited with 980 nm light to reveal an 800 nm emission image of the fingerprint. Fingerprints that have been dusted with upconversion material can be captured with no background fluorescence from the substrate, because not many materials fluoresce when excited with 980 nm light.

Utilizing NIR-to-Green UCNPs, or any other visible-light emitter, in ambient lighting can be difficult. Due to green peaks in ambient room lighting, there is a possibility that, with NIR-to-Green nanoparticles the emission peaks would be overshadowed by the background from the ambient light. Because there is no 800 nm emission in ambient room light, the NIR-to-NIR nanoparticles do not have this issue. Moreover, CCD-based cameras are significantly more sensitive to 800 nm light compared to visible light. This makes it easier to analyze fingerprints and reduces the intensity of excitation energy needed to do so.

In general, UCNPs exhibit low internal quantum efficiency, meaning that the ratio of photons emitted to photons absorbed is low. NIR-to-NIR UCNPs, however, appear to have a higher quantum efficiency relative to NIR-to-Green UCNPs. Upconversion efficiency is largely dictated by surface quenching and excitation irradiance. Surface quenching is effective because excitation energy migrates rapidly among Yb^{3+} ions to quenching sites on the surface of the nanoparticles. The use of protective shells, or passivation layers covers surface defects and shields optically active ions within the system, especially Yb^{3+}, from quenching solvent molecules and surface ligands. Usually these layers are made of inert material and therefore do not participate in upconversion. However, there have been instances where active shells have been untilized.[3] The active shell contains ions which participate in the excitation absorbance and energy transfer of the system that ultimately results in upconversion.
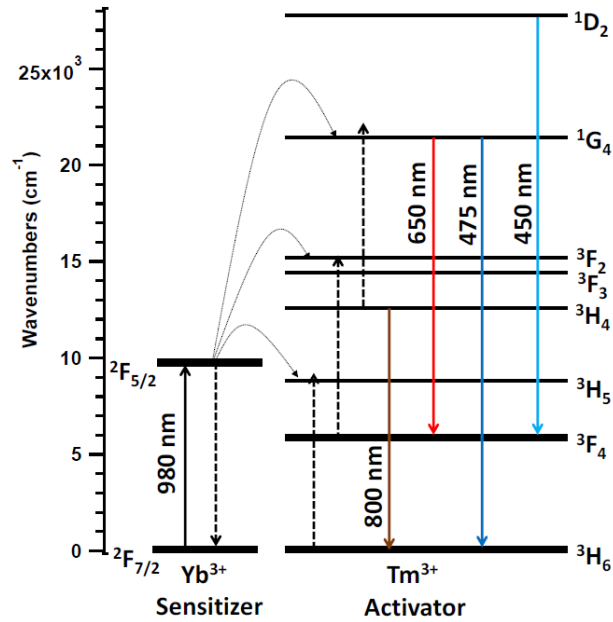
Figure 1. Energy transfer diagram between lanthanides in the NIR-to-NIR system

For over a decade, researchers have investigated NaYF$_4$: Yb, Er NIR-to-Green upconverting nanoparticles (UCNPs).[2,5-7,9,13] NaYF$_4$ doped with Yb and Er are called NIR-to-Green UCNPs, because they convert NIR excitation (980 nm) to 540 nm green emission (see Figure 2.). As with the NIR-to-NIR UCNPs, the Yb^{3+} ions act as sensitizers, the ions that absorb the excitation energy (980 nm). The energy absorbed by the Yb^{3+} ions is then transferred to nearby activator ions, in this case Er^{3+}. The energy is stored within the Er^{3+} ion long enough for the Yb^{3+}→Er^{3+} transfer to occur again. This results in a buildup of energy within the Er^{3+} ion promoting the Er^{3+} ion to higher and higher energy levels. This energy relaxation can result in 540 nm green ($^4S_{3/2} \rightarrow {}^4I_{15/2}$), 650 nm red ($^4F_{9/2} \rightarrow {}^4I_{15/2}$), and 1500 nm NIR ($^4I_{13/2} \rightarrow {}^4I_{15/2}$) emission.
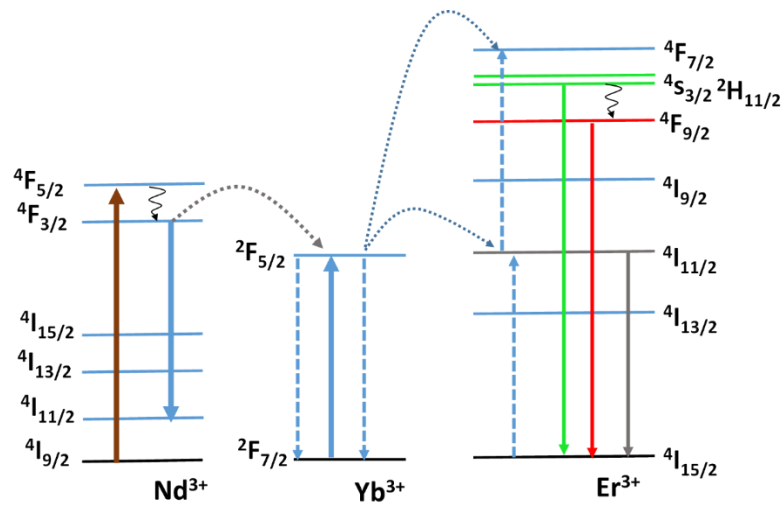
Figure 2. Energy transfer diagram between lanthanides in the NIR-to-Green system

NIR-to-Green UCNPs have important applications in a variety of fields, including bio-imaging, security printing, and latent fingerprint development.[1,3,11-13,15] Most upconverting nanoparticles are excited using 980 nm luminescence. 980 nm is within the transparent biological window (650-1350 nm) and can offer deep tissue penetration. However, water has a weak absorbance band that overlaps with the 980 nm excitation, weakening the upconversion luminescence. In addition to this, exciting NIR-to-Green UCNPs using 980 nm may also lead to overheating tissues. To avoid such issues, we have synthesized NIR-to-Green UCNPs that can be excited with 800 nm. By exciting UCNPs with 800 nm as opposed to 980 nm, we can decrease the chance of overheating tissue and circumvent any water interference.

In this project, β-NaYF$_4$: Yb, Er UCNPs with an active shell consisting of 10% Yb and 10% Nd were synthesized. The addition of the active Nd (sensitizer) shell allows for the

nanoparticles to be excited by 800 nm light. The Nd would then participate in energy transfer to Yb^{3+} ions (bridging sensitizer) and then to Er^{3+} ions (activator) (Figure 3).
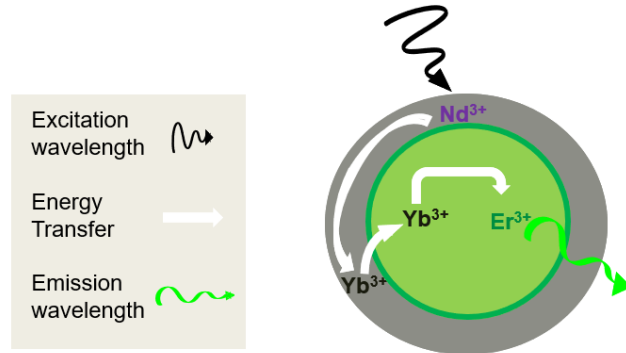
Figure 3. Energy transfer within NaYF$_4$: Yb, Er NIR-to-Green UCNPs with an active shell consisting of 10% Yb and 10% Nd

The Nd^{3+} ions absorb incoming 800 nm excitation and transfers the energy to a nearby Yb^{3+} ion which, like the NIR-to-NIR UCNPs, transfers the energy to the activator ions, Er^{3+}. The energy is stored within the Er^{3+} ion long enough for the Nd^{3+} →Yb^{3+} transfer to occur again. The additional photon of energy is again transferred to the Er^{3+} ion. This results in a buildup of energy within the Er^{3+} ion promoting the Er^{3+} ion to higher and higher energy levels. The core shell structure allows for successive $Nd^{3+} \rightarrow Yb^{3+} \rightarrow Er^{3+}$ energy transfer.

Exciting the particles with 800 nm, which is in a transparency window for biological samples, greatly reduces the danger of overheating tissue. For security printing, these particles can also be used to print two different but overlapping images which can be viewed individually using different excitation sources. Although these NIR-to-Green

UCNPs are advantageous for bio-imaging applications, they do have a weakness when used for latent fingerprinting development as discussed above.

Here, we aimed to increase the overall brightness of $NaYF_4$: Yb, Tm UCNPs by adjusting the Yb doping concentration and reducing the effect of surface quenching on the system by adding a passive shell. To do so, NIR-to-NIR UCNPs with varying Yb concentrations were synthesized. After UCNPs smaller than 100 nm were synthesized, inert shells of $NaYF_4$ were used to surround core particles to block the pathway of the energy migration to any surface quenchers while still maintaining the surface area to volume ratio. In addition to mitigating energy migration, the shells will also decrease the level of surface imperfections of the UCNPs. Adding shells around the UCNPs will result in an overall more efficient system.

Along with the work done on the NIR-to-NIR UCNPs, we also explored improving NIR-to-Green UCNPs for dual wavelength excitation. β-$NaYF_4$: Yb, Er with an active shell of $NaYF_4$: 10% Yb, 10% Nd were synthesized. In highly doped systems, concentration quenching is more likely to be a problem due to either non-radiative energy migration (Er^{3+}) to surface quenchers or cross-relaxation non-radiative energy loss. To solve this, UCNPs are usually synthesized with shell layers to reduce energy migration. The active shell permits these UCNPs to be excited by both 800 and 980 nm excitation. The active shell allows for not only dual wavelength excitation, but it subsequently curves the issue of concentration quenching too. The effect of the shell on overall brightness of the $NaYF_4$: Yb, Er NIR-to-Green was also observed.

In this chapter, the synthesis equipment and techniques used for this project are described in detail.

2.1 SYNTHESIS OF LANTHANIDE OLEATE PRECURSORS

To begin, lanthanide oxides, glacial acetic acid and DI water were added to a 500 mL 3-neck flask to convert the lanthanide oxides to lanthanide acetates. The solution was white and turbid. The solution was then left overnight to reflux at 102-104 °C. As the solution refluxed, it began to turn into a clear solution of lanthanide acetate. The following day, oleic acid was added, and the solution was placed under vacuum at 65 °C and then heated until the temperature was 105 °C. This is done to remove water from the reaction as the lanthanide oleates formed. The solution became clear and colorless as the temperature raised after the removal of water. Under controlled heating, the temperature was then raised from 105 °C to 132 °C to remove acetic acid. The reaction was then left stirring under 60 mTorr vacuum at 132 °C to reflux for at least an hour. After, the mixture was cooled to 100 °C while under vacuum. The vacuum was replaced with a light flow of N_2 gas. Once cooled, 1-octadecene was added to the solution under stirring.

2.2 SYNTHESIS OF β-NAYF$_4$ UCNPS

The green emitting UCNPs (β-NaYF$_4$:2%Er, 18%Yb) and NIR emitting UCNPs (β-NaYF$_4$:2%Tm, 48%Yb, β-NaYF$_4$:2%Tm, 58%Yb, and β-NaYF$_4$:2%Tm, 98%Yb) were synthesized according to the following procedure.

While stirring, an aqueous solution of NH_4F and NaOH was added to the lanthanide oleate precursor solutions described in Section 2.1. As the NaOH and NH_4F were added, the solution continued to cool to 43°C. The reaction was left stirring for another hour at 43°C. After one hour, vacuum was applied, and the reaction was heated. As a result of applying vacuum, the reaction mixture began to bubble as water was being taken out of the reaction. As soon as the formation of bubbles ceased, the temperature was increased to138°C. After an hour of heating at 138°C under 60 mTorr vacuum, the vacuum was replaced with a gentle flow of N_2 gas while the temperature was ramped to 320°C at a heating rate of 135% on a Variac transformer. As the reaction proceeded to 320°C the nucleation and growth mechanism involving the formation of small cubic (α) phase nanocrystals is induced. The α-phase nanocrystals undergo Ostwald ripening until portion of the α-phase nanocrystals surpass a size threshold. At this point the nanocrystals undergo a spontaneous phase change to the hexagonal (β) phase.[28] Due to the α-phase particles being more soluble than the β-phase particles, the solution is supersaturated relative to the β-phase. The β-phase seeds grow rapidly as the α-phase particles are dissolved.[29] The upconversion emission and temperature of the reaction mixture was monitored as described in Section 2.4. After completion, the reaction mixture was cooled to room temperature. The UCNPs were isolated and purified by three cycles of precipitation with acetone and subsequent re-dispersal in toluene. The UCNPs produced by this method are coated with oleate capping ligands, which facilitate adherence to fingerprint oils.

2.3 SHELL ADDITION

Two inert layers of $NaYF_4$ were added to a portion of the β-$NaYF_4$:2%Tm, 48%Yb (

resulting in $NaYF_4$:2%Tm, 48%Yb@$NaYF_4$ (core shell) and $NaYF_4$:2%Tm,

48%Yb@$NaYF_4$@$NaYF_4$ (core shell shell)) using a procedure of sacrificial α-$NaYF_4$

particles as shell stock; the α-$NaYF_4$ particles dissolve in the presence of β-phase core

particles and deposit onto the surface of the core particles as a β-phase shell in the

procedure described in Section 2.3.1 below. The inert shell contained no component that

exhibits upconversion.

An active shell layer of $NaYF_4$:10%Nd, 10%Yb was added to the β-$NaYF_4$:2%Er, 18%Yb

UCNPs. The active shell contained both Yb^{3+} and Nd^{3+} ions which both participate in the

upconversion of the system.

2.3.1 PREPARATION OF SACRIFICIAL α-$NaYF_4$ PARTICLES

A precursor of α-$NaYF_4$ particles was prepared similar to the procedure mentioned in

Section 2.1 with a few modifications. Yttrium oxide, glacial acetic acid and DI water were

added to a 500mL 3-neck flask to convert the lanthanide oxides to lanthanide acetates. The

solution was then left overnight to reflux at 102-104 °C. As the solution refluxed, it began

to turn into a clear solution of lanthanide acetate. The following day, oleic acid was added,

and the solution was placed under vacuum at 65 °C and then heated until the temperature

was 105 °C. This is done to remove water from the reaction as the lanthanide oleates

formed. The solution became clear and colorless as the temperature raised after the removal

of water. Under controlled heating, the temperature was then raised from 105 °C to 132 °C

to remove acetic acid. The reaction was then left stirring under 60 mTorr vacuum at 132

°C to reflux for at least an hour. After, the mixture was cooled to 100 °C while under

vacuum. The vacuum was replaced with a light flow of N_2 gas. Once cooled, 1-octadecene was added to the solution under stirring. While stirring, an aqueous solution of NH_4F and NaOH was added. As the NaOH and NH_4F were added, the solution continued to cool to 43°C. The reaction was left stirring for another hour at 43°C. After one hour, vacuum was applied, and the reaction was heated. As a result of applying vacuum, the reaction mixture began to bubble as water was being taken out of the reaction. As soon as the formation of bubbles ceased, the temperature was also increased to138°C. After two hours of heating at 138°C under 60 mTorr vacuum, the reaction was left to cool under ambient conditions and stored for later use.

Vacuum was applied and the reaction mixture heated from room temperature to 110 °C. At 110 °C the vacuum was replaced with a gentle flow of N_2 gas and reaction temperature was increased to 320 °C over an hour period. Temperature and emission were recorded as mentioned in section 2.4. Once the emission spectrum of the sample was stagnant, the reaction was left to cool to room temperature under stirring.

2.4　REAL-TIME MONITORING OF CORE AND CORE-SHELL UCNPS SYNTHESIS SETUP

A real-time setup, developed by Dr. John Sutter[28], was used to analyze the synthesis of the UCNPs as well as the addition of shells to the core UCNPs. This setup allows for temperature and emission spectrum of a reaction synthesis to be taken simultaneously as a function of time while the UCNPs are excited at 980 nm. The *in-situ* setup (Figure 4) includes a mobile laser unit with an 8 W continuous-wave 980 nm laser diode, a laptop connected to a miniature spectrometer connected to fiber-optic cable with a collecting lens, and a mounted filter. The filter is a 850 nm short pass filter was used for the NIR-to-NIR

UCNPs. This filter allows wavelengths shorter than 850 nm to pass through. This filter was discarded when monitoring the NIR-to-Green UCNPs. All of these were positioned in fixed spots for consistency. Images of temperature and emission profiles can be seen in Section 3.1.
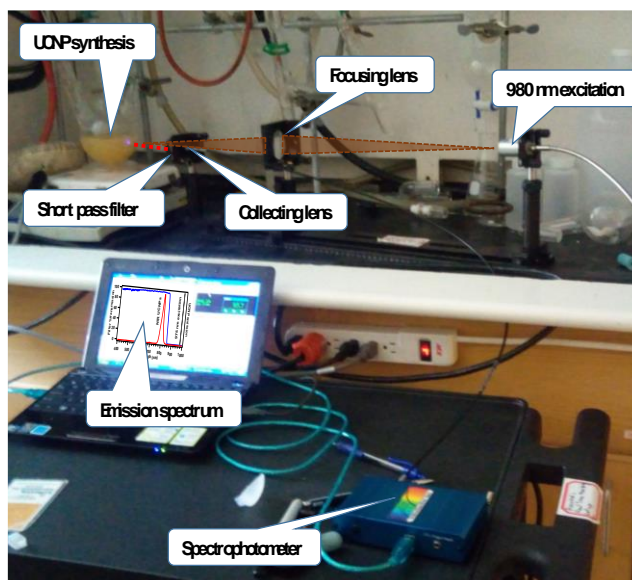

Figure 4. Real-time monitoring setup of UCNPs synthesis

2.5 NIR-TO-NIR UCNPS CLEANING AND PREPARATION FOR IMAGING AND SPECTROSCOPY

2 mL portions of NaYF$_4$: 48%Yb, 2%Tm core, NaYF$_4$: 48%Yb, 2%Tm@NaYF$_4$ core-shell, NaYF$_4$: 48%Yb, 2%Tm@NaYF$_4$@NaYF$_4$ core-shell-shell, NaYF$_4$: 58%Yb, 2%Tm, and NaYF$_4$: 98%Yb, 2%Tm UCNPs were each transferred into two separate 15 mL

12

centrifuge tubes. The UCNPs were precipitated with addition of 10 mL of acetone and centrifuged for 1 minute. The supernatant was decanted, and the precipitate was re-dispersed in 3 mL of toluene and sonication to form clear dispersions. To the dispersion, 10 mL of acetone was added to re-precipitates UCNPs and sonicated for an additional 5 minutes and centrifuged for 1 minute. The supernatant was decanted and one of the tubes was stored for reference. To the other tube, 5 mL of toluene was added, and UCNPs were dispersed in toluene using sonication for 5 minutes.

For SEM and TEM imaging (Section 3.2), in a glass vial, 0.1 mL of NIR-to-NIR UCNPs dispersions were added to 5 mL of toluene and sonicated for 10 minutes. This dilute dispersion of UCNPs was used to prepare samples for morphological studies.

For spectroscopy (Section 3.3.1), core samples were prepared by diluting 1 mL of UCNPs dispersion mentioned above, and additional 2 mL of toluene. The core-shell sample was prepared by diluting 2 mL of UCNPs dispersion and 1 mL of toluene, and core-shell-shell sample used the UCNPs dispersion from above without any further dilution.

2.6 NIR-TO-GREEN UCNPs CLEANING AND PREPARATION FOR IMAGING AND SPECTROSCOPY

2 mL of $NaYF_4$: 18%Yb, 2%Er core and 4 mL of $NaYF_4$: 18%Yb, 2%Er@ 10%Yb, 10%Nd core-shell raw, unwashed UCNPs were added to 2 separate,15 mL centrifuge tubes for washing. To each tube, ethanol was added to full the tubes to a volume of 14 mL. The tubes were inverted and shook several times to mix. They were then sonicated for 1 minute and centrifuged for 45 seconds at full speed (4500 RPM). The supernatant was decanted from

each tube. The particles were then dispersed by adding 3 mL of toluene to each tube. The tubes were sonicated for 30 seconds and agitated until fully suspended in solution. Once again, the tubes were filled with ethanol to 14 mL, inverted and shaken to mix, sonicated for 30 seconds, and centrifuged at full speed for 45 seconds. Supernatant was decanted. For the third wash, the nanoparticles were dispersed in 3mL of toluene, sonicated for 30 seconds, and agitated until fully suspended in solution. After fully dispersed, the volume was brought to 14 mL by adding acetone. The tubes were inverted and shaken to mix, sonicated for 30 seconds, and centrifuged at full speed for 45 seconds. Supernatant was decanted.

To one tube, 5 mL of toluene was added, and UCNPs were dispersed in toluene using sonication for 5 minutes. For SEM and TEM imaging (Section 3.4), in a glass vial, 0.1 mL of NIR-to-Green UCNPs dispersions were added to 5 mL of toluene and sonicated for 10 minutes. This dilute dispersion of UCNPs was used to prepare samples for morphological studies.

The second tube of the particles was then left uncapped to allow excess solvents to evaporate until they have dried to a hard-wet mass (~2 hours) and capped. 1 mL of carbon tetrachloride (CCl_4) was added to the tube of dried $NaYF_4$: 18%Yb, 2%Er core (100mg) and 1.5 mL of CCl_4 was added to the tube of dried $NaYF_4$: 18%Yb, 2%Er@ 10%Yb, 10%Nd core-shell (200mg) to disperse particles. The tube was sonicated for at least 30 seconds and centrifuged at 2000 RPM for ~45 seconds. Supernatants were collected for absorption and excitation spectroscopy seen in Section 3.3.2.

2.7 ELECTRON MICROSCOPY

A scanning electron microscope (SEM) with a field-emission source (Sigma FE-SEM; Zeiss) was used to characterize the size and morphology of the UCNPs.

2.8 SPECTROSCOPIC MEASUREMENTS

To determine the optical quality of the core and core-shell samples, we performed luminescence measurements on the nanocrystals. Time-resolved and steady-state spectroscopy was used to determine and compare 800 nm emission (NIR-to-NIR) and 540 nm (NIR-to-Green) intensity of the core and core-shell samples. The measurements were made using a 90° excitation-collection configuration with the nanocrystals dispersed in toluene in a 4 mm x 4 mm quartz cuvette. Through our measurements, we observed that the nanocrystals had a dispersion of high optical quality, with no discoloration. Following these measurements, emission spectra were taken using continuous wave (cw) excitation at 931 nm for the NIR-to-NIR UCNPs and 936.6 nm for the NIR-to-Green UCNPs. Lifetimes of the 1 µm emitting state of Yb^{3+} were taken using a pulsed optical parametric oscillator system, OPO, (Opolette HE 355 LD, Opotek, Inc) which was operated at 20 Hz (pulse width, FWHM < 7 ns; spectral linewidth= 4-7 cm^{-1}) and excited at 976 nm for both NIR-to-NIR and NIR-to-Green UCNPs. Excitation densities were approximated from the spot size of the laser and the measured laser power (Melles Griot 13PEM001). Spectra were obtained using a home-built system employing a 0.33m monochromator (iHR320, Horiba) and time-resolved photon counting techniques (SR430 multichannel scaler, SRS).

3.1 REAL-TIME MONITORING PROFILES OF UCNPS SYNTHESIS

Real-time monitoring profiles allows us to determine nanoparticle growth and temperature as a function of time. As temperature increases, the formation of α-phase nanoparticles takes place. As the α-phase continues to grow under constant heating, they undergo a thermodynamically driven a phase change (Oswald ripening) to β-phase nanoparticles. These β-phase nanoparticles are more energetically stable than the α-phase particles. The growth of β-phase nanoparticles leads to an increase of emission. Once the increase of emission begins to level out, it can be assumed that most of the α-phase nanoparticles have converted to β-phase nanoparticles and the reaction is completed.[28]

Using the setup described in Figure 4, we are able to simultaneously monitor the synthesis of UNCPs using temperature and emission as a function of time. Below in Figure 5 and 6, we have the real-time monitoring profiles of the synthesis of the $NaYF_4$: 48%Yb, 2%Tm core UCNPs and the addition of an inert shell on $NaYF_4$ to the $NaYF_4$:2%Tm, 48%Yb@$NaYF_4$ core-shell UCNPs respectively. The excitation wavelength was 980 nm and the monitored emission wavelength was 800 nm for each profile. For both the core and core-shell-shell the plots the black corresponds to the temperature as a function of time and the red is the intensity of 800 nm emission coming from the sample.

In the $NaYF_4$: 48%Yb, 2%Tm core synthesis profile (Figure 5) as temperature increases to 320°C over the span of 20 minutes. After the initial 20 minutes, the 800 nm emission from the 800 nm intensity decreased slightly as a result of the reduction of black body radiation

from the heating mantle. The reaction temperature remains constant at 320°C for an additional 40 minutes. After that, the 800 nm emission intensity from UCNP begins to increase and ultimately plateaus as time passes. Once the plateau in 800 nm emission is seen (at 80 minutes), we can conclude that the majority of the small cubic α-phase nanoparticles have dissolved and undergone Oswald ripening to convert to hexagonal β-phase nanoparticles. After the plateau was seen, the reaction mixture was taken off heat and cooled to room temperature.
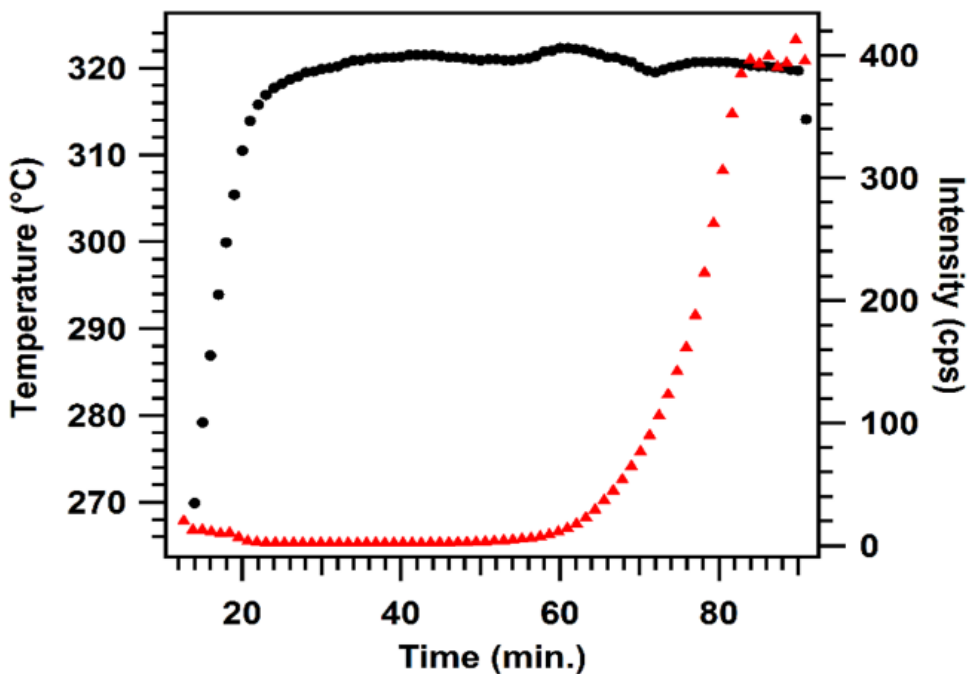

Figure 5.Real-time monitoring profile of NaYF$_4$: 48%Yb, 2%Tm core synthesis (λexc=980 nm and λem=800 nm).

With the core-shell-shell profile (Figure 6), the addition of an inert shell of NaYF$_4$ to NaYF$_4$: 48%Yb, 2%Tm@NaYF$_4$@NaYF$_4$ core-shell UCNPs was monitored. This resulted in the synthesis of NaYF$_4$: 48%Yb, 2%Tm@NaYF$_4$@NaYF$_4$ core-shell-shell

UCNPs. The first 10 minutes of the plot was a result of the excitation laser being off. From then on once the laser is on, we can see there was primordial 800 nm emission coming from the sample. Since the reaction mixture contained already synthesized β-NaYF$_4$:2%Tm, 48%Yb particles, we observed initial 800 nm emission from the sample. As the reaction temperature was increased to 310°C, beginning at 10 minutes, the 800 nm emission was decreased greatly, as a consequence of thermal quenching. After 35 minutes of heating at 310°C, the 800 nm emission from the reaction increased and began to plateau. Like the previously discussed core profile, we can conclude that the majority of the α-phase nanoparticles dissolved and deposited onto the β-phase NaYF$_4$ to NaYF$_4$: 48%Yb, 2%Tm@NaYF$_4$ core-shell nanoparticles.
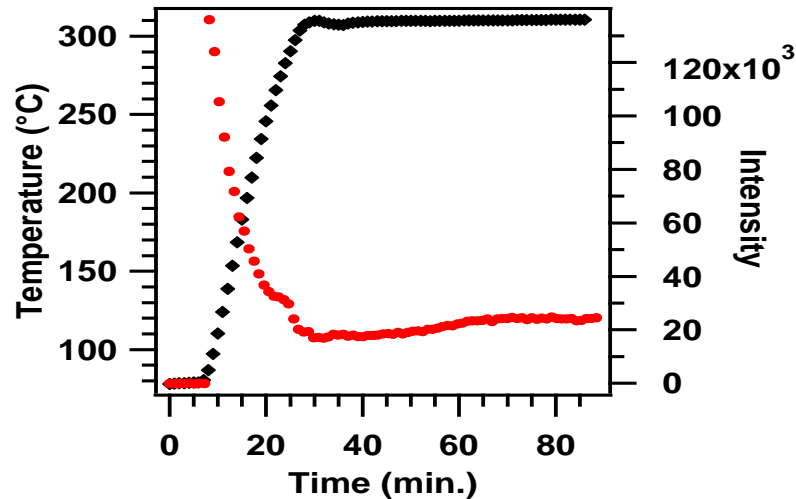
Figure 6.Real-time monitoring profile of the addition of an inert shell of NaYF$_4$ to NaYF$_4$: 48%Yb, 2%Tm@NaYF$_4$ core-shell UCNPs resulting in the synthesis of NaYF$_4$: 48%Yb, 2%Tm@NaYF$_4$@NaYF$_4$ core-shell-shell UCNPs (λexc=980 nm and λem=800 nm).

Below, Figure 7, is the real time monitoring profile of the addition of an inert NaYF$_4$ shell to NaYF$_4$: 18%Yb, 2%Er@Yb, Nd core-shell UCNPs resulting in the synthesis of NaYF$_4$:18%Yb, 2%Er@ 10%Yb, 10%Nd@ NaYF$_4$ UCNPs. Like the Figures 5 and 6, the

plot in black is the temperature as a function of time and the red monitors the intensity of emission, but for Figure 7 we are monitoring the 540 nm green emission. Previously, we monitored a similar reaction using 800 nm excitation, however due to extreme thermal quenching of the Nd, the monitoring was unsuccessful. Here we opted to excite using 980 nm to avoid quenching the Nd. Initially, while the reaction was being excited by a 980 nm laser there was some 540 nm emission. This is due to the core NIR-to-Green UCNPs being excited by the laser. However, we see that as temperature increased to 310°C, the 540 nm emission intensity begins decrease as a result of thermal quenching. After about one hour of consistent heating at 310°C, the 540 nm emission slowly decreased after 60 min of consistent heating at 310°C.This is unlike the previous profiles where an increase of 800 nm emission was seen along with a plateau of emission following shortly after. For this particular synthesis, as we continually heated the reaction, the reaction mixture turned black, decreasing the 540 nm emission. The reaction mixture was taken off heat and begins to cool, the 540 nm emission rises rapidly due to the reduction of thermal quenching.
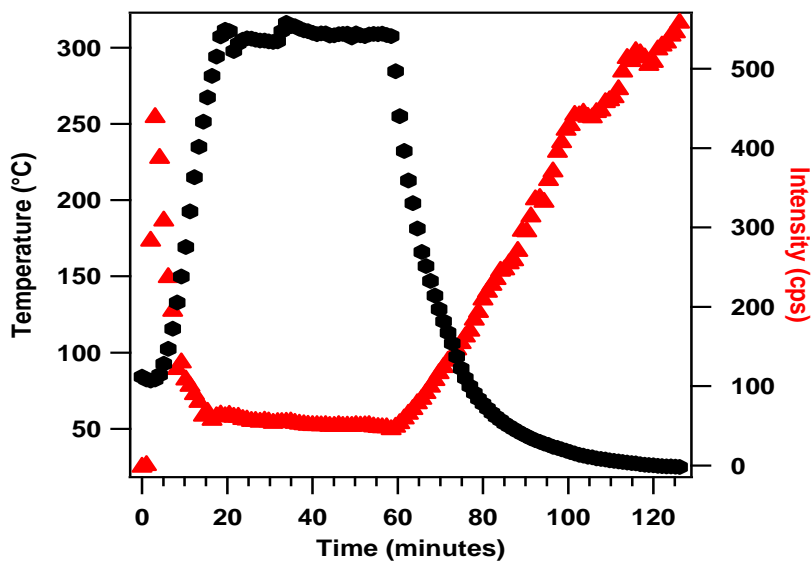
Figure 7. Real-time monitoring profile of an inert $NaYF_4$ shell addition to $NaYF_4$: 18%Yb, 2%Er@10%Yb, 10%Nd (λexc=980 nm and λem=540nm)

3.2 CRYSTAL SIZE AND MORPHOLOGY

Below is a comprehensive table (Table 1) detailing the size of the nanoparticles of 8 separate synthesis batches. All discussed UCNPs are hexagonal prisms. The edge-edge width is measured across the axial face of the nanoparticles and the length is measured along the c-axis which is perpendicular to the axial face of the nanoparticles.

Looking at entries 1 and 2, the addition of the inert $NaYF_4$ shell to the NIR-to-NIR UCNPs led to a shell thickness of 3.5 nm along the edge-edge width across axial face thickness of 4.5 nm along the length of c-axis, which resulted in an overall particle size of 48x49 nm and a shell thickness of 7x9 nm. This first addition was relatively uniform allowing the UCNPs to maintain their 1:1 surface ratio. The second inert shell addition seen in entry 3, resulted in an increase of the UCNPs size by 9x13 nm. The shell thickness along the edge-

edge width across axial face was 4.5 nm and 6.5 nm along the length of the c-axis. After the second shell addition, the nanoparticles became slightly oblong due to an uneven deposition of material onto the core-shell particles.

By adjusting the doping concentration of Yb for the NIR-to-NIR UCNPs, the size of the crystals can be somewhat controlled. With higher amounts of Yb, the nanocrystals increase in size. With higher amounts of Yb, the crystals become more plate like in shape compared to their usual hexagonal prism shape. These results are reflected in the size comparisons of the 58% Yb, 2% Tm core nanocrystals (entry 4) and the 98% Yb, 2% Tm core nanocrystals (entry 5) with the average size of a crystal being 132 nm and 259 nm along the axial face and 71 nm and 68 nm along the c-axis respectively (see Figure 8).

As for the NIR-to-Green UCNPs, comparing the core (entry 6) the addition of the first shell, an active shell consisting $NaYF_4$:10%Yb, 10%Nd (entry 7), resulted in a shell with an edge-edge width across axial face of 8.5 nm and 7.5 nm along the length of c-axis. The shell increased the overall size of the nanoparticles by 17x15 nm but maintained the 1:1 ratio of the core particles. After the synthesis of the active shell, a second inert shell was added to the NIR-to-Green UCNPs. We aimed for a particle increase of 5 nm (a shell thickness of 2.5 nm on both the axial face and along the c-axis) to preserve the 1:1 surface area ratio. However, after the second shell addition, the nanoparticles were found to have increased slightly on the axial face (thickness of 1.5 nm) and substantially along the c-axis (thickness of 15 nm). Overall, there was a 3x30 nm increase in size and a 1:2 surface ratio

for this batch of nanoparticles. Images of the NIR-to-Green UCNPs can be found in Figure

9.

Table 1. Dimensions of NIR-to-NIR UCNPs (entries 1-5) and NIR-to-Green UCNPs (entries 6-8) synthesized

Entry	Sample Name	Edge-Edge width across axial face (nm)	Length along c-axis (nm)
1	AR17MAY17 NIR- NaYF$_4$: 48%Yb, 2%Tm	48 ± 2	49 ± 3
2	AR19MAY17 NIR-NaYF$_4$:48%Yb, 2%Tm@NaYF$_4$ CS	55 ± 1	58 ± 3
3	AC06JUN17 NIR-NaYF$_4$:48%Yb, 2%Tm@NaYF$_4$ CSS	64 ± 2	71 ± 2
4	AC21JUN17 NIR- NaYF$_4$: 58%Yb, 2%Tm	132 ± 4	71 ± 2
5	AC10JUL17 NIR-NaYF$_4$: 98%Yb, 2%Tm	259 ± 8	68 ± 6
6	AC25JUN18 Green-NaYF$_4$: 18%Yb, 2%Er	40 ± 1	46 ± 2
7	AC29JUN18 Green-NaYF$_4$:18%Yb, 2%Er@ 10%Yb, 10%Nd CS	57 ± 2	61 ± 1
8	AC10JUL18 Green-NaYF$_4$:18%Yb, 2%Er@ 10%Yb, 10%Nd@ NaYF$_4$ CSS	60 ± 1	92 ± 1
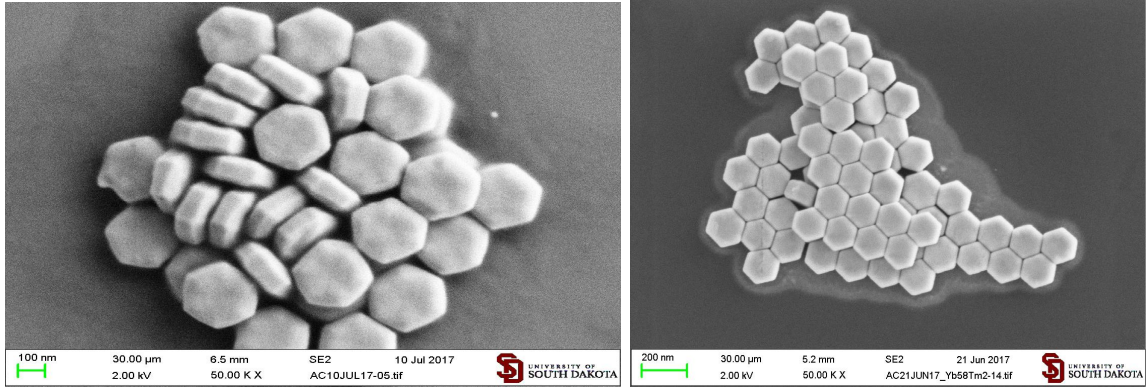
Figure 8. Left is an SEM image of NIR-to-NIR core NaYF$_4$:98% Yb, 2% nanocrystals (AC10JUL17). Right is an SEM image of NIR-to-NIR core NaYF$_4$:58% Yb, 2% Tm nanocrystals (AC21JUN17).
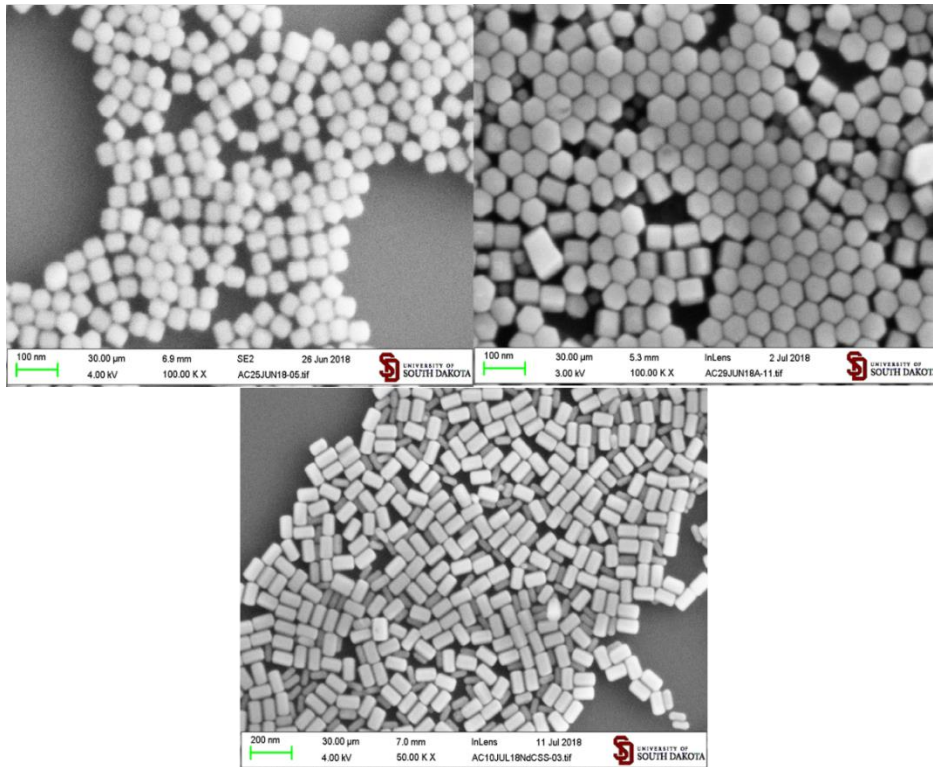

Figure 9. Top left is an SEM image of NIR-to-Green core NaYF$_4$: 18%Yb, 2%Er nanocrystals (AC25JUN18). Top right is an SEM image of NIR-to-Green core-shell NaYF$_4$:18%Yb, 2%Er@ 10%Yb, 10%Nd core-shell-shell nanocrystals (AC29JUN18). Bottom is an SEM image of NIR-to-Green NaYF$_4$:18%Yb, 2%Er@ 10%Yb, 10%Nd@NaYF$_4$ nanocrystals (AC10JUL18).

3.3 SPECTROSCOPY

3.3.1 NIR-TO-NIR UCNPS

Internal quantum efficiency (IQE) is defined as

Equation 1.

$$IQE = \frac{photons\ emitted}{photons\ absorbed}$$

Spectroscopic measurements described in Section 2.8 were used to determine IQE following a method described in the literature.[20] Because upconversion is a nonlinear process, IQE is dependent on the excitation flux. The measurements of the spectroscopic properties of the UCNPs were taken using a fixed experimental geometry and therefore the excitation flux becomes proportional to the intensity of the excitation beam. When using direct excitation into the emitting state, IQE can be calculated by obtaining the 1 μm decay curve of the UCNPs at a low power density to approximate a radiative decay constant of the 1 μm emission of Yb^{3+}.[20]

In Figure 10, we have plotted the IQE of 800 nm upconversion from core $NaYF_4$: 48%Yb, 2%Tm (red) and $NaYF_4$: 48%Yb, 2%Tm @$NaYF_4$@$NaYF_4$ core-shell-shell (blue) under various excitation power densities ranging from 1.5 to 14.5 W/cm^2 using 980 nm laser excitation and monitoring the 800 nm emission. From the data plotted in Figure 10, we see that the internal quantum efficiency of the core is much lower than the core-shell-shell sample measured at the same power density. The addition of passivation layers onto the $NaYF_4$: 48%Yb, 2%Tm core has a large effect on reducing surface quenching and increasing the overall IQE of the system.

To further quantify effect of the inert shell additions to the NaYF$_4$: 48%Yb, 2%Tm core

UCNPs enhancement factors (EF) were using Equation 2. below and plotted in Figure 11.

To calculate the EF, the ratio of the IQE of the NaYF$_4$: 48%Yb, 2%Tm@NaYF$_4$@NaYF$_4$

core-shell-shell and NaYF$_4$: 48%Yb, 2%Tm core was taken at the same power density.

Equation 2.

$$EF = \frac{IQE(core - shell - shell)}{IQE(core)}$$

The 800 nm emission from the NaYF$_4$: 48%Yb, 2%Tm @NaYF$_4$@NaYF$_4$ core-shell-shell

UCNPs at lowest power density, 1.5 W/cm^2, is more than 35 times brighter that the NaYF$_4$:

48%Yb, 2%Tm UCNPs at the same excitation density. The addition of an inert shell onto

the core NaYF$_4$: 48%Yb, 2%Tm nanoparticles increased the internal quantum efficiency

of the nanoparticles and brighter 800 nm emission from the nanocrystals when excited with

980 nm light.
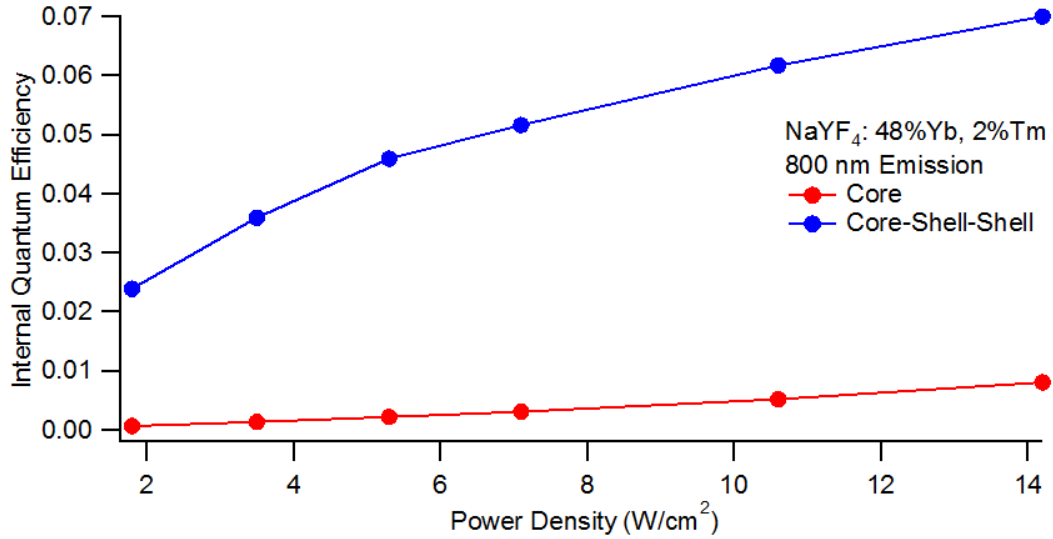
Figure 10. Internal quantum efficiency of 800 nm emission from NaYF$_4$: 48%Yb, 2%Tm core and core-shell-shell plotted as a function of power density. $IQE = \dfrac{photons\ emitted}{photons\ absorbed}$
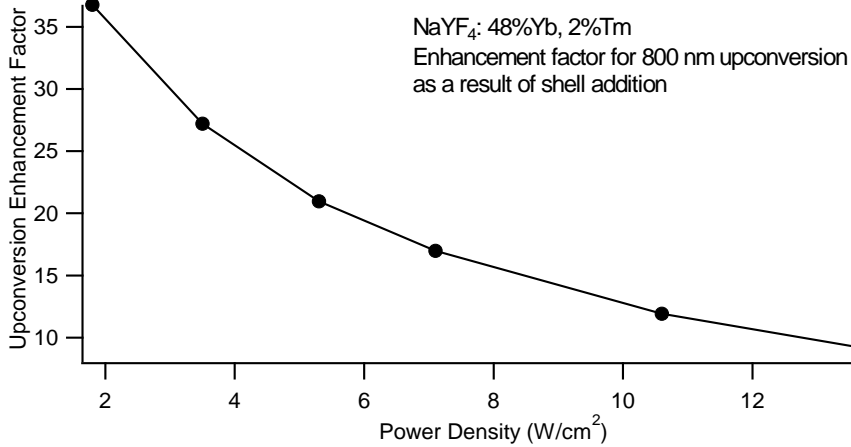
Figure 11. Enhancement factor for quantum efficiency increase in NIR-to-NIR UC resulting from shell addition vs excitation power density. $EF = \dfrac{QE(core\ shell\ shell)}{QE(core)}$

Figure 12 is a comparison of the 800 nm emission of NaYF$_4$: 48% Yb, 2% Tm@ NaYF$_4$@ NaYF$_4$ core-shell-shell, 48% Yb, 2% Tm@ NaYF$_4$ core-shell, NaYF$_4$: 48% Yb, 2% Tm core, NaYF$_4$: 58% Yb, 2% Tm, and NaYF$_4$: 98% Yb, 2% Tm UCNPs excited at 931 nm with varying power densities. The 800 nm emission of the UCNPs did increase with Yb

26

concentration, but the size of the higher doped UCNPs (NaYF$_4$: 58%Yb, 2% Tm, and NaYF$_4$: 98%Yb, 2% Tm) were much larger than 100 nm (see Table 1) and did not have a 1:1 surface ratio. Ultimately, passivation layers were added to NaYF$_4$: 48%Yb, 2% Tm core UCNPs to ensure that the resulting particles were smaller than 100 nm.
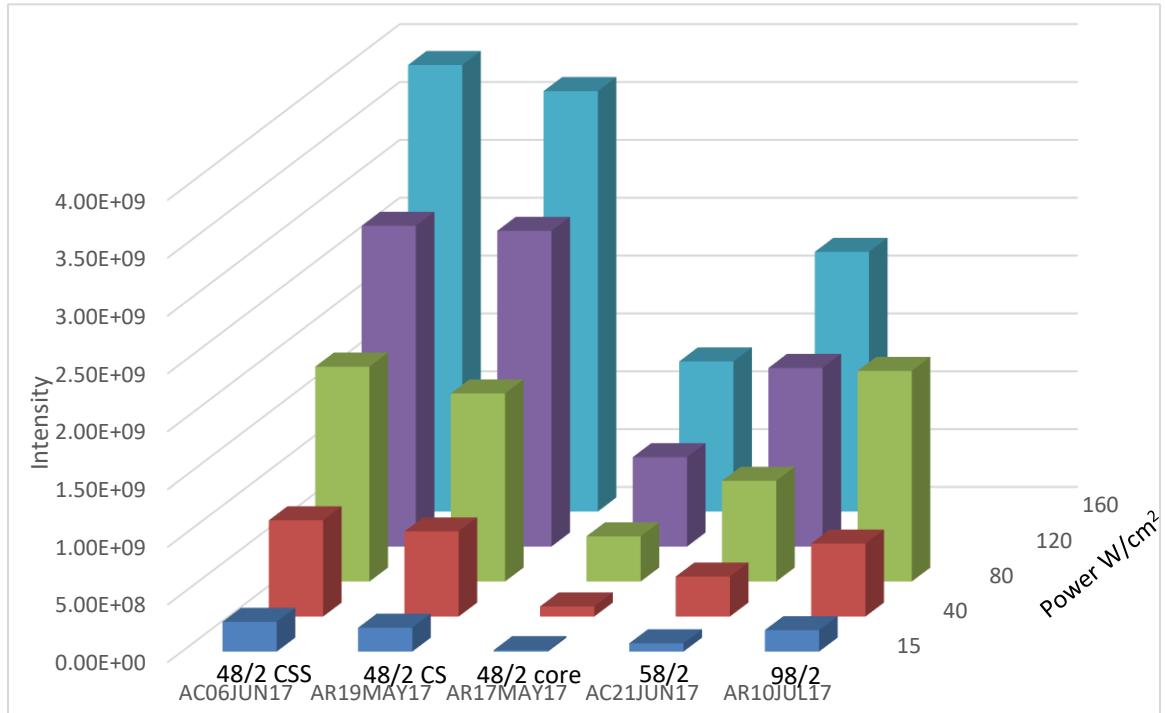
Figure 12. Comparison of NIR-to-NIR UCNPs 800 nm upconversion intensity at varying power densities (solutions were normalized for absorbance).

3.3.2 NIR-TO-GREEN UCNPS

Using the preparation mentioned above in Section 2.6, absorbance spectra both the NaYF$_4$: 18%Yb, 2%Er core and NaYF$_4$: 18%Yb, 2%Er@ 10%Yb, 10%Nd core-shell UCNPs were taken (Figure 13). The green spectrum is the core sample and the red the core-shell. The core sample a few, very weak, absorbance peaks and a large peak at 980 nm due to the Yb in the system. However, the core-shell spectrum has several large absorbance peaks at 520 nm, 580 nm, 760 nm, 860 nm, 980 nm and most importantly at 800 nm (Figure 13). From

this, we can conclude the presence of Nd and that the Nd was successfully synthesized onto

the UCNPs in the form of a shell.

Figure 13. Absorbance spectra of NaYF$_4$: 18%Yb, 2%Er core UCNPs (green) and NaYF$_4$: 18%Yb, 2%Er@ 10%Yb, 10%Nd core-shell UCNPs (red)

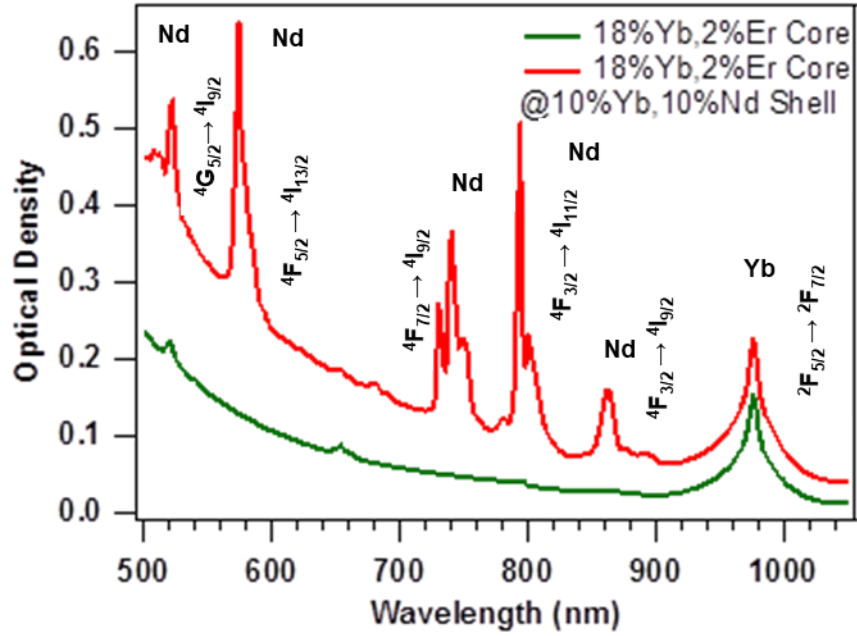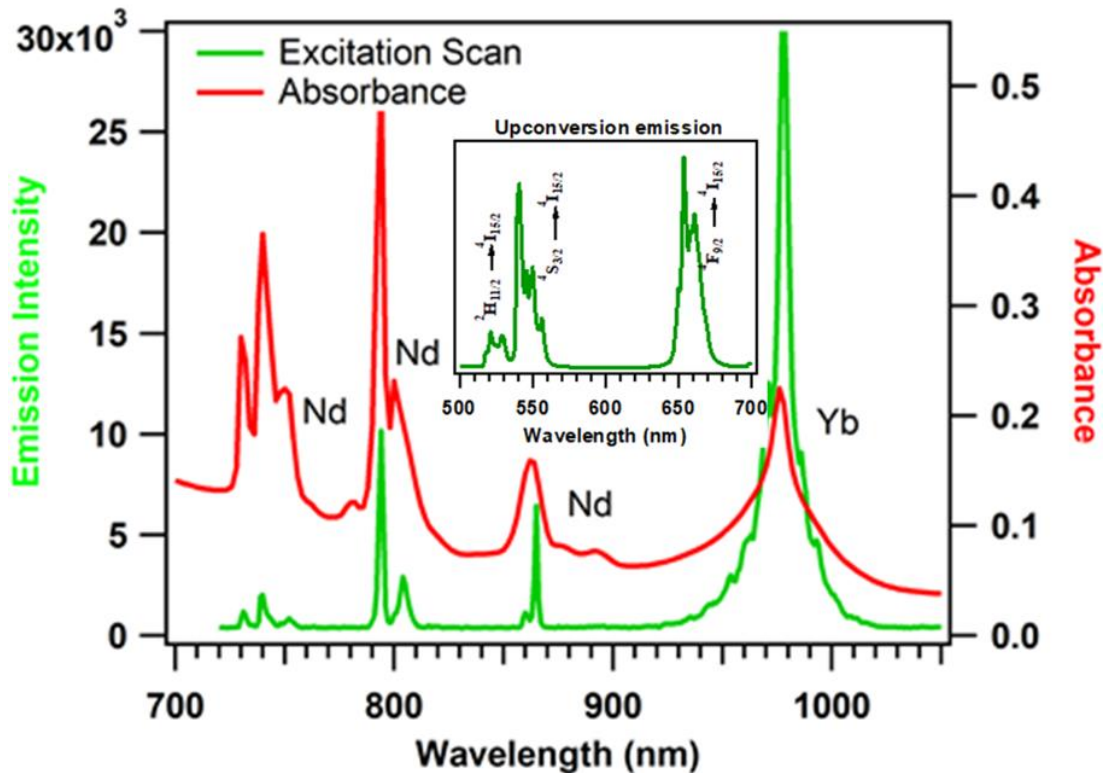Figure 14. Absorbance and excitation spectra (λem=540nm) of NaYF$_4$: 18%Yb, 2%Er@ 10%Yb, 10%Nd core-shell. Insert is the upconversion emission spectrum of NaYF$_4$: 18%Yb, 2%Er@ 10%Yb, 10%Nd CS UCNPs excited (λexc=976 nm).

Above (Figure 14) is the excitation (green) and absorbance (red) spectra of the of NaYF$_4$: 18%Yb, 2%Er@ 10%Yb, 10%Nd core-shell. Absorption is the absorbance of photons by the system. The excitation spectrum allows us to monitor the various bands of Nd, Er, and Yb that promotes upconversion. The absorption spectrum is similar to the excitation spectrum, yet the greater the absorbance at the excitation wavelength (936 nm) the more molecules are likely to be promoted to the excited state and more emission will be observed ($^2H_{11/2} \rightarrow {}^4I_{15/2}$). Here we can see that the absorbance and emission of peak size at 800 and 980 nm are switched. In the excitation spectrum, the 980 nm peak is much larger than the 800 nm peak. However, in the absorbance spectrum, the 800 nm peak appears to be larger

than the 980 nm peak. By comparing these two spectra, we can see that the Nd is more likely to absorb incoming excitation, but a smaller fraction of the absorbed photons contributes to UC compared to direct Yb excitation. The energy transfer from the Nd^{3+} $\rightarrow Yb^{3+}$ occurs, however the energy transfer from the $Yb^{3+} \rightarrow Er^{3+}$ does not arise as much. In other words, the IQE of the active shelled NIR-to-Green UCNPs is less than the IQE of the core NIR-to-Green UCNPs.
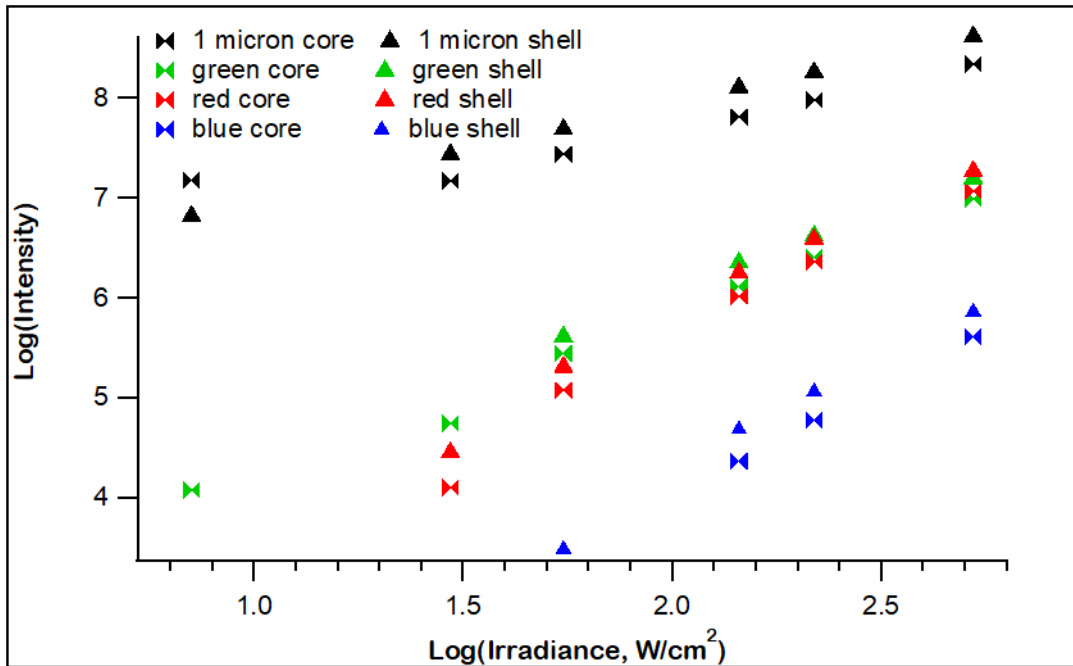
Figure 15. Plot comparing of $NaYF_4$: 18% Yb, 2% Er core (bowtie) and $NaYF_4$: 18% Yb, 2% Er@ 10% Yb, 10% Nd CS UCNP (triangle), 1 micron, green, red, and blue emission at various power densities.

In Figure 15, we are comparing the intensity of 1 micron, green, red, and blue emission of the $NaYF_4$: 18% Yb, 2% Er core and $NaYF_4$: 18% Yb, 2% Er@ 10% Yb, 10% Nd CS UCNPs as a function of irradiance. The slope of the lines to describe how sensitive the UCNPs emission is to the excitation power density. The higher the slope, the more sensitive the particles are.

30

4.1 NIR-TO-NIR UCNPS

For this project, three different batches of NIR-to-NIR UCNPs were synthesized with adjusted amounts of Yb, 48%, 58%, and 98% and fixed amount of Tm (2%). After measuring and each batch of nanoparticles, we concluded that with increasing levels of Yb, the particle dimensions increase from a 1:1 surface ratio to a 1:2 surface ratio, becoming plate-like. For the $NaYF_4$: 48%Yb, 2%Tm nanoparticles two separate inert shells of $NaYF_4$ were synthesized onto a portion of the batch. The luminescence of the $NaYF_4$: 48%Yb, 2%Tm core and $NaYF_4$: 48%Yb, 2% Tm@ $NaYF_4$@ $NaYF_4$ core-shell-shell were analyzed and compared using IQE measurements. As a result of the shell additions, the core-shell-shell UCNPs emit 800 nm light over 35 times that of the core UCNPs at low power densities (<1.5 W/cm^2). This is most likely due to the reduction of the surface quenching on the particles. The effectiveness of shell additions to the UCNPs systems will assist in further work to excited UCNPs at power densities comparable to LED lights. Extending the use of the NIR-to-NIR UCNPs with LED lights will further assist in implementing these powders in latent fingerprint development.

4.2 NIR-TO GREEN UCNPS

In this work, NIR-to-Green $NaYF_4$: 18%Yb, 2%Er UCNPs were synthesized with the addition of a 10%Yb, 10%Nd active shell and an inert shell of $NaYF_4$. It was found through the absorbance and excitation spectra of the core-shell NIR-to-Green particles that the Nd of the $NaYF_4$: 18%Yb, 2%Er@ 10%Yb, 10%Nd core-shell UCNPs is more likely than the Nd to act as the initial sensitizer in the system and absorb the incoming photon. However,

Yb is most probable to participate in energy transfer of the photons. Although IQE measurements were not recorded with the NIR-to-Green UCNPs, we still saw an increase in 540 nm emission (Figure 13). Like the previously discussed NIR-to-NIR UCNPs, the addition of a(n) (active) shell to the NIR-to-Green UCNPs resulted in brighter overall emission when compared to the core counterpart. The core-shell NIR-to-Green UCNPs were also successfully excited at both 800 nm and 980 nm. The inert shelled batch of NIR-to-Green UCNPs were synthesized, but we have yet to analyze their emission. There is still future work to be done to further explore the upconversion capabilities of the active shelled NIR-to-Green UCNPs. We hope to utilize their duel wavelength excitability for increasing anticounterfeiting measures.

1   Agrawal, S.; Dubey, V., Down conversion luminescence behavior of Er and Yb doped Y_2O_3 phosphor. *Journal of Radiation Research and Applied Sciences* **2014,** *7* (4), 601-606.

2   Chen, J.; Guo, C.; Wang, M.; Huang, L.; Wang, L.; Mi, C.; Li, J.; Fang, X.; Mao, C.; Xu, S., Controllable synthesis of $NaYF_4$: Yb,Er upconversion nanophosphors and their application to in vivo imaging of Caenorhabditis elegans. *Journal of Materials Chemistry* **2011,** *21* (8), 2632-2638.

3   Estebanez, N.; Ferrera-González, J.; Francés-Soriano, L.; Arenal, R.; González-Béjar, M.; Pérez-Prieto, J., Breaking the Nd^{3+}-sensitized upconversion nanoparticles myth about the need of onion-layered structures. *Nanoscale* **2018,** *10* (26), 12297-12301.

4   Fond, B.; Abram, C.; Pougin, M.; Beyrau, F., Characterisation of dispersed phosphor particles for quantitative photoluminescence measurements. *Optical Materials* **2019,** *89*, 615-622.

5   Fujii, M.; Nakano, T.; Imakita, K.; Hayashi, S., Upconversion Luminescence of Er and Yb Codoped $NaYF_4$ Nanoparticles with Metal Shells. *The Journal of Physical Chemistry C* **2013,** *117* (2), 1113-1120.

6   Geitenbeek, R. G.; Prins, P. T.; Albrecht, W.; van Blaaderen, A.; Weckhuysen, B. M.; Meijerink, A., $NaYF_4:Er^{3+},Yb^{3+}/SiO_2$ Core/Shell Upconverting Nanocrystals for Luminescence Thermometry up to 900 K. *The Journal of Physical Chemistry C* **2017,** *121* (6), 3503-3510.

7   Hu, D.; Chen, M.; Gao, Y.; Li, F.; Wu, L., A facile method to synthesize superparamagnetic and up-conversion luminescent $NaYF_4:Yb, Er/Tm@SiO_2@Fe_3O_4$ nanocomposite particles and their bioapplication. *Journal of Materials Chemistry* **2011,** *21* (30), 11276-11282.

8   Huang, X., Dual-model upconversion luminescence from $NaGdF_4:Nd/Yb/Tm@NaGdF_4:Eu/Tb$ core–shell nanoparticles. *Journal of Alloys and Compounds* **2015,** *628*, 240-244.

9   Jacobsohn, L. G.; Sprinkle, K. B.; Kucera, C. J.; James, T. L.; Roberts, S. A.; Qian, H.; Yukihara, E. G.; DeVol, T. A.; Ballato, J., Synthesis, luminescence and scintillation of rare earth doped lanthanum fluoride nanoparticles. *Optical Materials* **2010,** *33* (2), 136-140.

10   Johnson, N. J. J.; He, S.; Nguyen Huu, V. A.; Almutairi, A., Compact Micellization: A Strategy for Ultrahigh T1 Magnetic Resonance Contrast with Gadolinium-Based Nanocrystals. *ACS Nano* **2016,** *10* (9), 8299-8307.

11   Johnson, N. J. J.; Oakden, W.; Stanisz, G. J.; Scott Prosser, R.; van Veggel, F. C. J. M., Size-Tunable, Ultrasmall $NaGdF_4$ Nanoparticles: Insights into Their T1 MRI Contrast Enhancement. *Chemistry of Materials* **2011,** *23* (16), 3714-3722.

12   Kamkaew, A.; Chen, F.; Zhan, Y.; Majewski, R. L.; Cai, W., Scintillating Nanoparticles as Energy Mediators for Enhanced Photodynamic Therapy. *ACS Nano* **2016,** *10* (4), 3918-3935.

13   Kang, X.; Cheng, Z.; Li, C.; Yang, D.; Shang, M.; Ma, P. a.; Li, G.; Liu, N.; Lin, J., Core–Shell Structured Up-Conversion Luminescent and Mesoporous $NaYF_4:Yb^{3+}/Er^{3+}@nSiO_2@mSiO_2$ Nanospheres as Carriers for Drug Delivery. *The Journal of Physical Chemistry C* **2011,** *115* (32), 15801-15811.

14   Khan, I.; Saeed, K.; Khan, I., Nanoparticles: Properties, applications and toxicities. *Arabian Journal of Chemistry* **2017**.

15   Klier, D. T.; Kumke, M. U., Upconversion NaYF 4: Yb: Er nanoparticles co-doped with Gd $^{3+}$ and Nd $^{3+}$ for thermometry on the nanoscale. *Rsc Advances* **2015,** *5* (82), 67149-67156.

16   Li, Z.; Wang, L.; Wang, Z.; Liu, X.; Xiong, Y., Modification of $NaYF_4:Yb,Er@_{SiO2}$ Nanoparticles with Gold Nanocrystals for Tunable Green-to-Red Upconversion Emissions. *The Journal of Physical Chemistry C* **2011,** *115* (8), 3291-3296.

17   Li, Z.; Zhang, Y.; Jiang, S., Multicolor Core/Shell-Structured Upconversion Fluorescent Nanoparticles. *Advanced Materials* **2008,** *20* (24), 4765-4769.

18. Lu, F.; Yang, L.; Ding, Y.; Zhu, J.-J., Highly Emissive Nd3+-Sensitized Multilayered Upconversion Nanoparticles for Efficient 795 nm Operated Photodynamic Therapy. *Advanced Functional Materials* **2016,** *26* (26), 4778-4785.

19. Würth, C.; Fischer, S.; Grauel, B.; Alivisatos, A. P.; Resch-Genger, U., Quantum Yields, Surface Quenching, and Passivation Efficiency for Ultrasmall Core/Shell Upconverting Nanoparticles. *Journal of the American Chemical Society* **2018,** *140* (14), 4922-4928.

20. May, P. S.; Baride, A.; Hossan, M. Y.; Berry, M., Measuring the internal quantum yield of upconversion luminescence for ytterbium-sensitized upconversion phosphors using the ytterbium(iii) emission as an internal standard. *Nanoscale* **2018,** *10* (36), 17212-17226.

21. Niu, W.; Wu, S.; Zhang, S., A facile and general approach for the multicolor tuning of lanthanide-ion doped NaYF4 upconversion nanoparticles within a fixed composition. *Journal of Materials Chemistry* **2010,** *20* (41), 9113-9117.

22. Niu, W.; Wu, S.; Zhang, S.; Li, J.; Li, L., Multicolor output and shape controlled synthesis of lanthanide-ion doped fluorides upconversion nanoparticles. *Dalton Transactions* **2011,** *40* (13), 3305-3314.

23. Noculak, A.; Podhorodecki, A., Size and shape effects in β-NaGdF4: Yb^{3+}, Er^{3+} nanocrystals. *Nanotechnology* **2017,** *28* (17), 175706.

24. Rasskazov, I.; Wang, L.; Murphy, C.; Bhargava, R.; Carney, P., Plasmon-enhanced upconversion: Engineering enhancement and quenching at nano and macro scales. *Optical Materials Express* **2018,** *8*, 3787.

25. Reddy, K. L.; Prabhakar, N.; Arppe, R.; Rosenholm, J. M.; Krishnan, V., Microwave-assisted one-step synthesis of acetate-capped NaYF4:Yb/Er upconversion nanocrystals and their application in bioimaging. *Journal of Materials Science* **2017,** *52* (10), 5738-5750.

26. Rinkel, T.; Raj, A. N.; Dühnen, S.; Haase, M., Synthesis of 10 nm β-NaYF4:Yb,Er/NaYF4 Core/Shell Upconversion Nanocrystals with 5 nm Particle Cores. *Angewandte Chemie International Edition* **2016,** *55* (3), 1164-1167.

27. Rodrigues, E. M.; Gálico, D. A.; Lemes, M. A.; Bettini, J.; T. Neto, E.; Mazali, I. O.; Murugesu, M.; Sigoli, F. A., One pot synthesis and systematic study of the photophysical and magnetic properties and thermal sensing of α and β-phase NaLnF4 and β-phase core@shell nanoparticles. *New Journal of Chemistry* **2018,** *42* (16), 13393-13405.

28. Suter, J. D.; Pekas, N. J.; Berry, M. T.; May, P. S., Real-Time-Monitoring of the Synthesis of β-NaYF4:17% Yb,3% Er Nanocrystals Using NIR-to-Visible Upconversion Luminescence. *The Journal of Physical Chemistry C* **2014,** *118* (24), 13238-13247.

29. May, P. B.; Suter, J. D.; May, P. S.; Berry, M. T., The Dynamics of Nanoparticle Growth and Phase Change During Synthesis of β-NaYF4. *The Journal of Physical Chemistry C* **2016,** *120* (17), 9482-9489.

30. Tessitore, G.; Mandl, G. A.; Brik, M. G.; Park, W.; Capobianco, J. A., Recent insights into upconverting nanoparticles: spectroscopy, modeling, and routes to improved luminescence. *Nanoscale* **2019,** *11* (25), 12015-12029.

31. Vargas, J. M.; Blostein, J. J.; Sidelnik, I.; Brito, D. R.; Palomino, L. A. R.; Mayer, R. E., Luminescent and scintillating properties of lanthanum fluoride nanocrystals in response to gamma/neutron irradiation: codoping with Ce activator, Yb wavelength shifter, and Gd neutron captor. *Journal of Instrumentation* **2016,** *11* (09), P09007-P09007.

32. Wang, L.; Li, Y., Controlled Synthesis and Luminescence of Lanthanide Doped NaYF4 Nanocrystals. *Chemistry of Materials* **2007,** *19* (4), 727-734.

33. Wang, M.; Abbineni, G.; Clevenger, A.; Mao, C.; Xu, S., Upconversion nanoparticles: synthesis, surface modification and biological applications. *Nanomedicine* **2011,** *7* (6), 710-29.

34   Wang, M.; Li, M.; Yang, M.; Zhang, X.; Yu, A.; Zhu, Y.; Qiu, P.; Mao, C., NIR-induced highly sensitive detection of latent fingermarks by NaYF$_4$:Yb,Er upconversion nanoparticles in a dry powder state. *Nano Research* **2015,** *8* (6), 1800-1810.

35   Wang, M.; Li, M.; Yu, A.; Wu, J.; Mao, C., Rare Earth Fluorescent Nanomaterials for Enhanced Development of Latent Fingerprints. *ACS Applied Materials & Interfaces* **2015,** *7* (51), 28110-28115.

36   Weber, M. J., Scintillation: mechanisms and new crystals. *Nuclear Instruments and Methods in Physics Research Section A: Accelerators, Spectrometers, Detectors and Associated Equipment* **2004,** *527* (1-2), 9-14.

37   Wei, W.; Chen, G.; Baev, A.; He, G. S.; Shao, W.; Damasco, J.; Prasad, P. N., Alleviating Luminescence Concentration Quenching in Upconversion Nanoparticles through Organic Dye Sensitization. *Journal of the American Chemical Society* **2016,** *138* (46), 15130-15133.

38   Wen, S., Zhou, J., Zheng, K. *et al.* Advances in highly doped upconversion nanoparticles. *Nat Commun* **9,** 2415 **2018**. https://doi.org/10.1038/s41467-018-04813-5

39   Hongli, W.; Hai, Z.; Xian, C.; Fu, H. T.; Beilei, W.; Guangyu, Z.; Fung, Y. S.; Feng, W., Upconverting Near-Infrared Light through Energy Management in Core–Shell–Shell Nanoparticles. *Angewandte Chemie International Edition* **2013,** *52* (50), 13419-13423.

40   Xie, X.; Gao, N.; Deng, R.; Sun, Q.; Xu, Q.-H.; Liu, X., Mechanistic Investigation of Photon Upconversion in Nd3+-Sensitized Core–Shell Nanoparticles. *Journal of the American Chemical Society* **2013,** *135* (34), 12608-12611.

41   Xu, B.; Zhang, X.; Huang, W.; Yang, Y.; Ma, Y.; Gu, Z.; Zhai, T.; Zhao, Y., Nd3+ sensitized dumbbell-like upconversion nanoparticles for photodynamic therapy application. *Journal of Materials Chemistry B* **2016,** *4* (16), 2776-2784.

42   Ye-Fu Wang, Gao-Yuan Liu, Ling-Dong Sun, Jia-Wen Xiao, Jia-Cai Zhou, and Chun-Hua Yan *ACS Nano* **2013** 7 (8), 7200-7206

43   Zhan, Q.; Wang, B.; Wen, X.; He, S., Controlling the excitation of upconverting luminescence for biomedical theranostics: neodymium sensitizing. *Optical Materials Express* **2016,** *6* (4), 1011-1023.

44   Zhang, Y.; Yu, Z.; Li, J.; Ao, Y.; Xue, J.; Zeng, Z.; Yang, X.; Tan, T. T. Y., Ultrasmall-Superbright Neodymium-Upconversion Nanoparticles via Energy Migration Manipulation and Lattice Modification: 808 nm-Activated Drug Release. *ACS Nano* **2017,** *11* (3), 2846-2857.

45   Zhao, J.; Sun, Y.; Kong, X.; Tian, L.; Wang, Y.; Tu, L.; Zhao, J.; Zhang, H., Controlled Synthesis, Formation Mechanism, and Great Enhancement of Red Upconversion Luminescence of NaYF$_4$:Yb^{3+}, Er^{3+} Nanocrystals/Submicroplates at Low Doping Level. *The Journal of Physical Chemistry B* **2008,** *112* (49), 15666-15672.

46   Yeteng, Z.; Gan, T.; Zhanjun, G.; Yijun, Y.; Lin, G.; Yuliang, Z.; Ying, M.; Jiannian, Y., Elimination of Photon Quenching by a Transition Layer to Fabricate a Quenching-Shield Sandwich Structure for 800 nm Excited Upconversion Luminescence of Nd^{3+}-Sensitized Nanoparticles. *Advanced Materials* **2014,** *26* (18), 2831-2837.